INNOVATION FOREVER
Open Access

Innovation Discovery

ISSN 2959-5150 (Online)

Short Communication

Examining the Impact of Initial Stress on a Micro-elongated Thermoelastic Medium Immersed in an Unbounded Inviscid Fluid Under Two Theoretical Models

Mohamed F. Ismail[1], **Hamdy M. Ahmed**[2], **Homan Emadifar**[3*], **Karim K. Ahmed**[4]

[1]*Faculty of Computers and Information System, Egyptian Chinese University, Cairo, Egypt*
[2]*Department of Physics and Engineering Mathematics, Higher Institute of Engineering, El Shorouk Academy, Cairo, Egypt*
[3]*Department of Basic Sciences, Technical and Vocational University (TVU), Tehran, Iran*
[4]*Department of Mathematics, Faculty of Engineering, German International University (GIU), New Administrative Capital, Cairo, Egypt*

[*]***Correspondence to: Homan Emadifar, PhD,*** *Department of Basic Sciences, Technical and Vocational University (TVU), Tehran, Iran; Email: homan_emadi@yahoo.com*

Abstract

In this paper, a detailed investigation is carried out into the dynamic behavior of a micro-elongated thermoelastic half-space submerged within an infinite, inviscid (non-viscous) fluid medium, while accounting for the effects of initial stress. The analysis focuses on two distinct thermoelastic theories: the Lord-Shulman (L-S) model and the Dual-Phase-Lag (DPL) model. Within this framework, the governing equations for the system are rigorously formulated based on both theoretical approaches. An analytical solution to the problem is obtained through the application of the normal mode analysis technique. To illustrate and compare the impact of initial stress on the micro-elongated thermoelastic medium interacting with the surrounding fluid, an aluminum epoxy is chosen as the material under consideration. The results derived under the L-S theory are systematically compared against those obtained using the DPL model to highlight differences in the material's response. The comprehensive analysis demonstrates that initial stress exerts a profound influence on the behavior of all studied physical fields, including displacement, temperature, micro-elongated distribution, and stress components.'

Keywords: thermoelasticity, normal mode, initial stress, micro-elongation

Received: April 23, 2025
Revised: June 1, 2025
Accepted: July 15, 2025
Published: August 4, 2025

Citation: Ismail MF, Ahmed HM, Emadifar H, Ahmed KK. Examining the Impact of Initial Stress on a Micro-elongated Thermoelastic Medium Immersed in an Unbounded Inviscid Fluid under two Theoretical Models. *Innov Discov*, 2025; 2(3): 14.

1 INTRODUCTION

In a pivotal contribution in 2002, Quintanilla[1] rigorously established that the governing equation within the Dual-Phase-Lag (DPL) theory of heat conduction admits well-posed solutions and exhibits continuous dependence on the prescribed initial conditions. Subsequently, in 2006, Quintanilla and Racke[2,3] conducted a comprehensive comparative study of the two distinct hyperbolic heat conduction models formulated by Tzou under the DPL framework. Within the same year, these researchers further extended their investigation to encompass the DPL-based thermoelasticity models independently introduced by Chandrasekharaiah and Tzou. Through mathematical analysis, they revealed that the corresponding solution sets are governed by a semigroup of contractions, thereby confirming the stability and solvability of the models under appropriate functional settings. Complementing these foundational studies, Roy-Choudhuri[4] explored the influence of the DPL model in the context of thermoelastic wave propagation within a one-dimensional elastic half-space, highlighting the model's capacity to capture phase-lag-induced dispersion phenomena. Building upon the theoretical refinement of Fourier's law through DPL considerations, numerous subsequent studies[5-11] have emerged, contributing significantly to the advancement of the field by exploring various applications and extensions of DPL-based heat conduction and thermoelastic models in complex physical settings.

Within this broader framework, a micro-elongated elastic medium is characterized by four degrees of freedom: three translational motions and one micro-elongation mode. In such materials, in addition to classical deformation, material points may experience volumetric micro-elongation, meaning they can expand or contract independently of translational motion. Examples of such materials include solid-liquid crystals, fiber-reinforced composites, and porous media saturated with non-viscous fluids or gases. Research into functionally graded micro-elongated media was pioneered by Shaw and Mukhopadhyay[12], who examined how material properties and thermoelastic coefficients varying exponentially with distance affect material behavior. Their subsequent work[13] extended this to analyze how moving heat sources influence infinitely long, isotropic, and homogeneous micro-elongated thermoelastic solids using generalized thermoelastic theories. Further advancements were made by Ailawalia and Sachdeva[14], who investigated how internal heat sources affect deformation within a micro-elongated layer beneath a finite elastic layer. Later, Ailawalia and Pathania[15] studied similar effects but for a micro-elongated layer situated below an infinite elastic layer, applying the Green-Lindsay framework. Additionally, Ailawalia and Singla[16] explored two-dimensional deformations arising from laser pulse heating in a micro-elongated thermoelastic layer of thickness $2d$. Significant contributions were also made by Othman[17,18], who examined the propagation of thermoelastic disturbances in semiconductor materials with temperature-dependent properties within the DPL model. His work demonstrated how initial stress and temperature variations can fundamentally alter wave propagation dynamics in isotropic elastic media, providing crucial insights into high-precision materials engineering.

In recent work, I explored a range of modern computational and analytical techniques applied across various nonlinear and fractional-order models in mathematical physics and biomedicine. Key topics included stochastic computing approaches for modeling HIV prevention dynamics and supervised neural network methods for simulating fractional-order Leptospirosis models, demonstrating the potential of machine learning in epidemic modeling. I also discussed fluid dynamics and heat transfer in nanofluids, focusing on thin film flow of Cu-nanofluids over stretching sheets with slip and convective boundary conditions — an area closely related to heat conduction mechanisms in thermoelastic materials. Further, I presented analytical and numerical investigations into solitary wave behaviors in nonlinear evolution equations such as the Chaffee–Infante and perturbed Fokas–Lenells equations, and how these techniques are instrumental in understanding wave propagation, a fundamental aspect of thermoelasticity. Additionally, I examined blood flow simulation in stenotic arteries using hybrid nanofluids with silver and gold nanoparticles, offering biomedical analogs to thermal stress and material response in complex domains. Finally, the talk covered the modulation instability and optical wave dynamics in higher-dimensional Schrödinger-type models and introduced new soliton solutions to nonlinear M-fractional evolution equations in shallow water contexts, for more details see[19-26]. These studies collectively underscore the synergy between thermoelasticity and computational wave dynamics, enriching our understanding of material behavior under coupled thermal and mechanical influences.

In the realm of advanced thermoelastic analysis, significant developments have emerged through various sophisticated modeling frameworks. The ATSS model, built upon the Cattaneo-Christov thermal framework, provides a refined understanding of entropy-optimized ternary nanomaterial flow, especially under the influence of homogeneous-heterogeneous chemical reactions, enhancing the coupling between thermal relaxation and microstructural diffusion. Concurrently, the incorporation of modified thermal and solutal fluxes in the convective flow of Reiner–Rivlin materials offers deeper insight into viscoelastic behavior under non-Fourier heat conduction. The HARK formulation extends the scope by integrating entropy generation into convective transport processes beyond constant thermophysical properties, thereby addressing variable material behavior under thermoelastic deformation. The SAT approach, grounded in a modified Cattaneo–Christov framework, facilitates the modeling of entropy-generating hybrid nanomaterial flows, capturing the complexity of dual-phase lag effects in heterogeneous systems. Furthermore, the TASA formulation, dedicated to nonlinear radiative flows of Walter–B nanoliquids with suspended microorganisms, integrates bio-convective mechanisms and entropy generation into the generalized thermoelastic perspective, for mor details see[27-32]. Collectively, these models enrich the theoretical and practical understanding of thermoelastic responses in nanofluidic systems, particularly in the presence of heat flux memory, nonlinear radiation, and chemically reactive environments.

In the present study, we direct our focus toward investigating the thermoelastic behavior of a micro-elongated thermoelastic half-space immersed within an infinitely extending, inviscid (non-viscous) fluid medium under the influence of pre-existing initial stress, as schematically illustrated in Figure 1. The analysis is conducted within the framework of two fundamental theoretical models: DPL model and the Lord-Shulman (L-S) theory. The research commences with a detailed derivation and presentation of the governing equations characterizing the physical behavior of the system. To simplify the complex mathematical structure and make the problem dimensionally consistent, we introduce a non-dimensionalization process, reformulating the

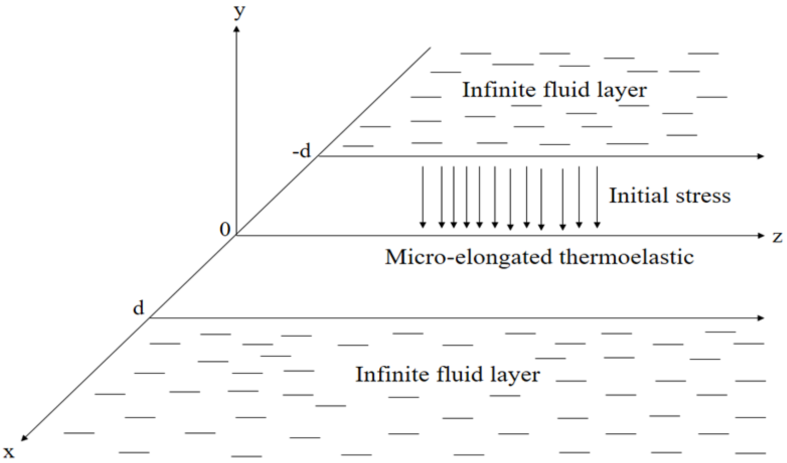

Figure 1. Geometry of the Problem.

governing relations into a dimensionless form. This step not only generalizes the findings but also reduces computational complexity. Subsequently, to facilitate the analytical solution process, we apply the normal mode analysis technique. This method transforms the original set of partial differential equations (PDEs) into corresponding ordinary differential equations (ODEs), which are more manageable and suitable for solution within the considered geometry. Following the transformation, boundary conditions are carefully formulated and imposed at the interface These boundary conditions are essential for determining the integration constants that emerge within the general solutions of the differential equations. By rigorously applying these conditions, a complete and consistent solution to the problem is achieved. Finally, the theoretical findings are substantiated through numerical simulations. We perform detailed numerical computations to illustrate the physical implications of the developed models. The obtained results are systematically analyzed, discussed, and represented graphically to provide a clear visualization of the influence of initial stress on various thermoelastic and microstructural fields within the medium.

2 METHODS

2.1 Basic Equations

The system of governing equations of a micro-elongated thermoelasticity with initial stress in a DPL model can be written as[15,17]

$$\sigma_{ij,j} = \rho u_{i,tt} \tag{1}$$

$$a_0 \varphi_{,ii} + \beta_1 T - \lambda_1 \varphi - \lambda_0 u_{j,j} = \frac{1}{2} \rho j_0 \varphi_{,tt} \tag{2}$$

$$k\left(1+\tau_\theta \frac{\partial}{\partial t}\right) T_{,ii} = \left(1+\tau_q \frac{\partial}{\partial t}\right) \left(\rho c_e \frac{\partial T}{\partial t} + \beta_0 T u_{k,kt}\right) + \beta_1 T_0 \varphi_{,t} \tag{3}$$

$$\sigma_{ij} = 2\mu \varepsilon_{ij} + (\lambda e - \beta_0 T + \lambda_0 \varphi)\delta_{ij} - P(\delta_{ij} - w_{ij}) \tag{4}$$

Where $w_{ij} = \frac{1}{2}(u_{j,i} - u_{i,j})$

From Equations (1) and (4) for displacement vector and the initial stress, (P) the equations of motion are given by

$$(\lambda+\mu) e_{,x} + \mu \nabla^2 u_1 - \frac{P}{2}(u_{1,zz} - u_{3,xz}) + \lambda_0 \varphi_{,x} - \beta_0 T_{,x} = \rho u_{1,tt} \tag{5}$$

$$(\lambda+\mu) e_{,z} + \mu \nabla^2 u_3 - \frac{P}{2}(u_{3,xx} - u_{1,xz}) + \lambda_0 \varphi_{,z} - \beta_0 T_{,z} = \rho u_{3,tt} \tag{6}$$

For simplicity, the following non-dimensional variables are used

$$\begin{gathered} x_i' = \frac{w^*}{c_1} x_i, z' = \frac{w^*}{c_1} z, u_i' = \frac{w^* \rho c_1}{\beta_0 T_0} u_i, \\ u_i^{e'} = \frac{w^* \rho c_1}{\beta_0 T_0} u_i^e, t' = w^* t, \tau_\theta' = w^* \tau_\theta, \tau_q' = w^* \tau_q, \\ \sigma_{ij}' = \frac{\sigma_{ij}}{\beta_0 T_0}, \sigma_{ij}^{e'} = \frac{\sigma_{ij}^e}{\beta_0 T_0}, \varphi' = \frac{\lambda_0}{\beta_0 T_0} \varphi, \\ T' = \frac{T}{T_0}, P' = \frac{P}{\lambda + 2\mu}, P_1' = \frac{P_1}{\beta_0 T_0} \end{gathered} \tag{7}$$

Where, $w^* = \frac{\rho c_1^2 c_e}{k}, c_1^2 = \frac{\lambda + 2\mu}{\rho}$.

Substituting from Equation (7) into Equations (2), (3), (5), and (6), we obtain

$$a_2 e_{,x} + a_1 \nabla^2 u_1 + \frac{P}{2}(u_{1,zz} - u_{3,xz}) + \varphi_{,x} - T_{,x} = u_{1,tt} \tag{8}$$

$$a_2 e_{,z} + a_1 \nabla^2 u_3 + \frac{P}{2}(u_{3,xx} - u_{1,xz}) + \varphi_{,z} - T_{,z} = u_{3,tt} \tag{9}$$

$$-a_5 e + (\nabla^2 - a_4)\varphi + a_3 T = a_6 \varphi_{,tt} \tag{10}$$

$$(1 + \tau_\theta \frac{\partial}{\partial t}) \nabla^2 T = (1 + \tau_q \frac{\partial}{\partial t})[a_7 T_{,t} + a_8 e_{,t}] + a_9 \varphi_{,t} \tag{11}$$

2.2 Normal Mode Analysis

The solution of the physical variable recognized may be analysed in normal modes as the following form:

$$[u_i, \varphi, T, \sigma_{ij}, u_i^f, \sigma_{ij}^f](x,z,t) = [u_i^*, \varphi^*, T^*, \sigma_{ij}^*, u_i^{f*}, \sigma_{ij}^{f*}](z) e^{(wt+ibx)} \tag{12}$$

Where is a complex constant, $i = \sqrt{-1}$, is wave number in the *x* direction.

Using Equation (12) into Equations (8-11), then we have

$$ib\varphi^* + [\delta_1 D^2 - \delta_2] u_1^* - ibT^* + \delta_3 D u_3^* = 0 \tag{13}$$

$$D\varphi^* + \delta_3 D u_1^* - DT^* + [\delta_4 D^2 - \delta_5] u_3^* = 0 \tag{14}$$

$$[D^2 - \delta_7]\varphi^* - \delta_6 u_1^* + a_3 T^* - a_5 D u_3^* = 0 \tag{15}$$

$$\delta_{13}\varphi^* + \delta_{10}u_1^* - [\delta_8 D^2 - \delta_{12}]T^* + \delta_{11}Du_3^* = 0 \ (16)$$

Equations (13-16) have a non-trivial solution if the physical quantities' determinant coefficients equal to zero, then we get.

$$(D^8 - AD^6 + BD^4 - CD^2 + E)u_1^*(z), u_3^*(z), T^*(z), \varphi^*(z) = 0 (17)$$

Equation (18) can be factorized as:

$$\begin{gathered}(D^2 - k_1^2)(D^2 - k_2^2)(D^2 - k_3^2)(D^2 - k_4^2) \\ u_1^*(z), u_3^*(z), T^*(z), \varphi^*(z) = 0\end{gathered} \quad (18)$$

Where, are roots of the characteristic equation of Equation (18).

The general solutions of Equation (18) bound as is given by

$$\begin{gathered}(u_1^*, u_3^*, T^*, \varphi^*)(z) = \sum_{n=1}^{4}(1, H_{1n}, H_{2n}, H_{3n})M_n e^{k_n z} \\ + \sum_{n=1}^{4}\left(1, H_{1(n+4)}, H_{2(n+4)}, H_{3(n+4)}\right)M_{(n+4)}e^{-k_n z}\end{gathered} \quad (19)$$

Substituting from Equation (7) into Equation (4), and with the help of Equation (19), we obtain the components of stresses.

$$\begin{gathered}(\sigma_{xx}, \sigma_{zz})(z) = \sum_{n=1}^{4}(H_{4n}, H_{5n})M_n e^{(k_n z + wt + ibx)} \\ + \sum_{n=1}^{4}\left(H_{4(n+4)}, H_{5(n+4)}\right)M_{n+4}e^{(-k_n z + wt + ibx)} - a_{11}P,\end{gathered} \quad (20)$$

$$\begin{gathered}\sigma_{xz}(z) = \sum_{n=1}^{4} H_{6n}M_n e^{(k_n z + wt + ibx)} \\ + \sum_{n=1}^{4} H_{6(n+4)}M_{n+4}e^{(-k_n z + wt + ibx)},\end{gathered} \quad (21)$$

Where the coefficient a_i, δ_i, A, B, C, E, and are given in Appendix 1.

The basic equation in the fluid is given by Othman and Ismail[33]

$$\lambda^f \nabla(\nabla . u^f) = \rho^f u^f_{,tt}, \ (22)$$

$$\sigma^f_{ij} = \lambda^f u^f_{r,r}\delta_{ij}. \quad (23)$$

Substituting from Equation (12) into Equation (22)

$$\left(\frac{w^2}{(c_1^f)^2} - b^2\right) u_1^{*f} + ibDu_3^{*f} = 0 \ (24)$$

$$\left(D^2 + \frac{w^2}{(c_1^f)^2}\right) u_3^{*f} + ibDu_1^{*f} = 0 \ (25)$$

Where, $c_1^{f^2} = \frac{\lambda^f}{\rho^f}$.

Eliminating between Equations (24) and (25), we obtain

$$[\ D^2 - r^2\ ]\left(u_1^{*f},\ u_3^{*f}\right) = 0 \ (26)$$

The root of the auxiliary equation of Equation (26) is and the solution of Equation (26) has the form

$$\left(\bar{u}_1^f,\ \bar{u}_3^f\right)(z) = (1,\ L_{11})R_1\ e^{rz} + (1,\ L_{12})R_2 e^{-rz} (27)$$

Substituting from Equation (12) in Equation (23) and by using Equation (27), we acquire the stress components in a fluid layer.

$$\sigma_{xx}^{*f}(z) = \sigma_{yy}^{*f}(z) = \sigma_{zz}^{*f}(z) = L_{21}R_1 e^{rz} + L_{22}R_2 e^{-rz} (28)$$

Where,

$$L_{11} = \frac{-ibr}{\left[r^2 + \frac{w^2}{(c_1^f)^2}\right]}, L_{12} = \frac{i\ b\ r}{\left[r^2 + \frac{w^2}{(c_1^f)^2}\right]}, L_{21} = \lambda^f[ib + rL_{11}], L_{22} = \lambda^f[ib - rL_{12}].$$

2.3 Boundary Conditions

To find the constants and we have applied boundary conditions for this problem at $z=\pm d$,

$$\begin{gathered}\sigma_{xx} = \sigma_{xx}^f, \sigma_{xz} = f_1 e^{ib(x-\xi t)}, \frac{\partial u_1}{\partial z} = \frac{\partial u_1^f}{\partial z}, \\ \varphi = 0, T = f_2 e^{ib(x-\xi t)}. \text{ at } z = \pm\ d\end{gathered} \quad (29)$$

Using the expressions for and in Equation (29), we get

$$\begin{gathered}
\sum_{n=1}^{4} H_{4n}M_n e^{k_n d} + \sum_{n=1}^{4} H_{4(n+4)}M_{n+4}e^{-k_n d} - L_{22}R_2 e^{-rd} = a_{11}P, \\
\sum_{n=1}^{4} H_{4n}M_n e^{-k_n d} + \sum_{n=1}^{4} H_{4(n+4)}M_{n+4}\ e^{k_n d} - L_{21}R_1\ e^{-rd} = a_{11}P, \\
\sum_{n=1}^{4} H_{6n}M_n e^{k_n d} + \sum_{n=1}^{4} H_{6(n+4)}M_{n+4}\ e^{-k_n d} = f_1, \\
\sum_{n=1}^{4} H_{6n}M_n e^{-k_n d} + \sum_{n=1}^{4} H_{6(n+4)}M_{n+4}\ e^{k_n d} = f_1, \\
\sum_{n=1}^{4} k_n M_n e^{k_n d} - \sum_{n=1}^{4} k_n M_{n+4}e^{-k_n d} + rR_2 e^{-rd} = 0, \\
\sum_{n=1}^{4} k_n M_n e^{-k_n d} - \sum_{n=1}^{4} k_n M_{n+4}e^{k_n d} - rR_1 e^{-rd} = 0, \\
\sum_{n=1}^{4} H_{3n}M_n\ e^{k_n d} + \sum_{n=1}^{4} H_{3(n+4)}M_{n+4}\ e^{-k_n d} = 0, \\
\sum_{n=1}^{4} H_{3n}M_n\ e^{-k_n d} + \sum_{n=1}^{4} H_{3(n+4)}M_{n+4}\ e^{k_n d} = 0, \\
\sum_{n=1}^{4} H_{2n}M_n\ e^{k_n d} + \sum_{n=1}^{4} H_{2(n+4)}M_{n+4}\ e^{-k_n d} = f_2, \\
\sum_{n=1}^{4} H_{2n}M_n\ e^{-k_n d} + \sum_{n=1}^{4} H_{2(n+4)}M_{n+4}\ e^{k_n d} = f_2
\end{gathered} \quad (30)$$

By solving the system of non-homogeneous Equations (30), the constants M_{n+4}, R_1 and can be obtained, then, we define the distribution of all the field quantities.

3 RESULTS AND DISCUSSION

The analysis is conducted for aluminum epoxy-like material as[13]:

$$\begin{gathered}
\beta_0 = \beta_1 = 0{,}05 \times 10^5 N/m^2.k, c_e = 966J/kg.k, k = 252J/m.s.k, \\
j_0 = 0.196 \times 10^{-4}m^2, \lambda = 7.59 \times 10^{10}N/m^2, \mu = 1.89 \times 10^{10}N/m^2, \\
a_0 = 0.61 \times 10^{-10}N, \rho = 2.19 \times 10^3\text{kg}/m^3, \lambda_0 = \lambda_1 = 0.37 \times 10^{10}N/m^2, \\
T_0 = 293k, P = 0.001, \tau_\theta = 1.5 \times 10^{-4}, \tau_q = 9 \times 10^{-4}, w = w_0 + i\zeta, \\
w_0 = -1.77 \times 10^{-4}, \zeta = 3.59 \times 10^{-3}, b = 3, f_1 = 0.025, f_2 = 0.025
\end{gathered}$$

As a non-viscous fluid, water has the physical constants are given by Othman and Ismail[33]

$$\lambda^f = 2.25 \times 10^9 N.m^{-2}, \rho^f = 10^3 kg.m^{-3}$$

In this paper, the calculations are carried out to a value dimensionless time t=1.02 in the range on the surface x=0.5. The numerical strategy stated herein is used to distribute horizontal displacement u_1, vertical displacement u_3, temperature , micro-elongational scalar φ,stresses components σ_{xx}, σ_{zz}, and against distance z (Figure 2A-G). To study the effect of the presence and complete absence of initial stress in the DPL model and L-S. This paper introduces the results of the numerical assessment in the form of a graph. Figure 2A presents the variation of the horizontal displacement as a function of the spatial or temporal variable, comparing two different cases: the presence and the complete absence of initial stress. It is observed that the presence of initial stress significantly influences the displacement profile, causing either amplification or suppression of the displacement depending on the region. The curve corresponding to the case with initial stress generally exhibits sharper gradients and higher amplitudes, indicating the role of initial stress in modifying the wave propagation characteristics and material deformation. Figure 2B illustrates the variation of the vertical displacement under two scenarios: with and without initial stress. The curves show that initial stress affects the magnitude and distribution of vertical displacement through the material. In regions where mechanical or thermal gradients are prominent, the presence of initial stress appears to either enhance or reduce the displacement compared to the stress-free case. This behavior highlights the anisotropic effects introduced by initial stresses, influencing the vertical motion of material particles during thermoelastic interactions. Figure 2C shows the temperature distribution is plotted for both the presence and absence of initial stress. The curves reveal that the initial stress not only affects the mechanical response but also has a noticeable impact on thermal fields. Specifically, temperature diffusion and the resulting thermal gradients are altered in the stressed material. The figure suggests that initial stress can either accelerate or delay the thermal response, depending on its nature (compressive or tensile), thus impacting heat conduction in the thermoelastic medium. Figure 2D shows the variation of the micro-elongational scalar with and without initial stress. The micro-elongation, which represents internal structural deformations at the micro-scale, is significantly influenced by the pre-existing stress state. In the stressed case, shows distinct peaks or troughs, indicating enhanced microstructural activity. The comparison suggests that initial stress plays a crucial role in micro-mechanical processes and might lead to more complex internal deformation patterns within the material. Figure 2E shows the force stress component (normal stress in the x-direction) is plotted for both cases. It is clear from the figure that initial stress affects the stress distribution within the material. The stressed configuration exhibits higher peak values and sharper transitions in the stress field compared to the unstressed case. These observations underline how initial stress modifies internal forces, potentially leading to different failure modes or stability conditions in thermoelastic bodies. Figure 2F depicts the variation of the force stress component (normal stress in the z-direction). Similar to the horizontal stress component, the vertical stress shows distinct differences between the stressed and unstressed states. In the presence of initial stress, the material experiences either elevated or reduced stress concentrations depending on the location. The behavior of reflects how the initial conditions influence vertical load-bearing capacity and mechanical equilibrium. figure, the variation of the force stress component (shear stress component) is presented. The curves indicate that initial stress significantly modifies the shear stress distribution. Regions of stress concentration or relaxation differ markedly between the two cases, demonstrating the complex interplay between initial stresses and thermoelastic shear deformations. The shear component is particularly sensitive to initial stress, highlighting its role in dictating the onset of shear instabilities or potential slip surfaces within the material (Figure 2G).

4 CONCLUSION

In this study, a comprehensive analytical investigation was conducted to examine the influence of initial stress on a micro-elongated thermoelastic half-space submerged within an infinite non-viscous fluid, employing the DPL model and the L-S theory. By deriving the governing equations, applying non-dimensionalization, and utilizing the normal mode analysis, the problem was systematically transformed from a set of PDEs into ODEs, enabling precise analytical treatment. The effects of initial stress were incorporated explicitly into the formulation, and the boundary conditions were carefully applied at the interface to determine the constants arising in the solution. Numerical simulations were performed to visualize and compare the behavior of various physical quantities, including displacements, temperature distribution, and stress components, under the presence and absence of initial stress. The results clearly demonstrate that initial stress has a significant and profound impact on the thermoelastic and microstructural responses of the material. Under both the DPL and L-S models, initial stress was found to alter the amplitude, phase, and propagation characteristics of thermal and mechanical waves within the medium. Furthermore, comparisons between the DPL and L-S theories revealed that the inclusion of phase-lag effects in the DPL model provides a more detailed description of the material's response, particularly in capturing the finite speed of heat propagation and the time-delay phenomena in heat and mechanical wave interactions.

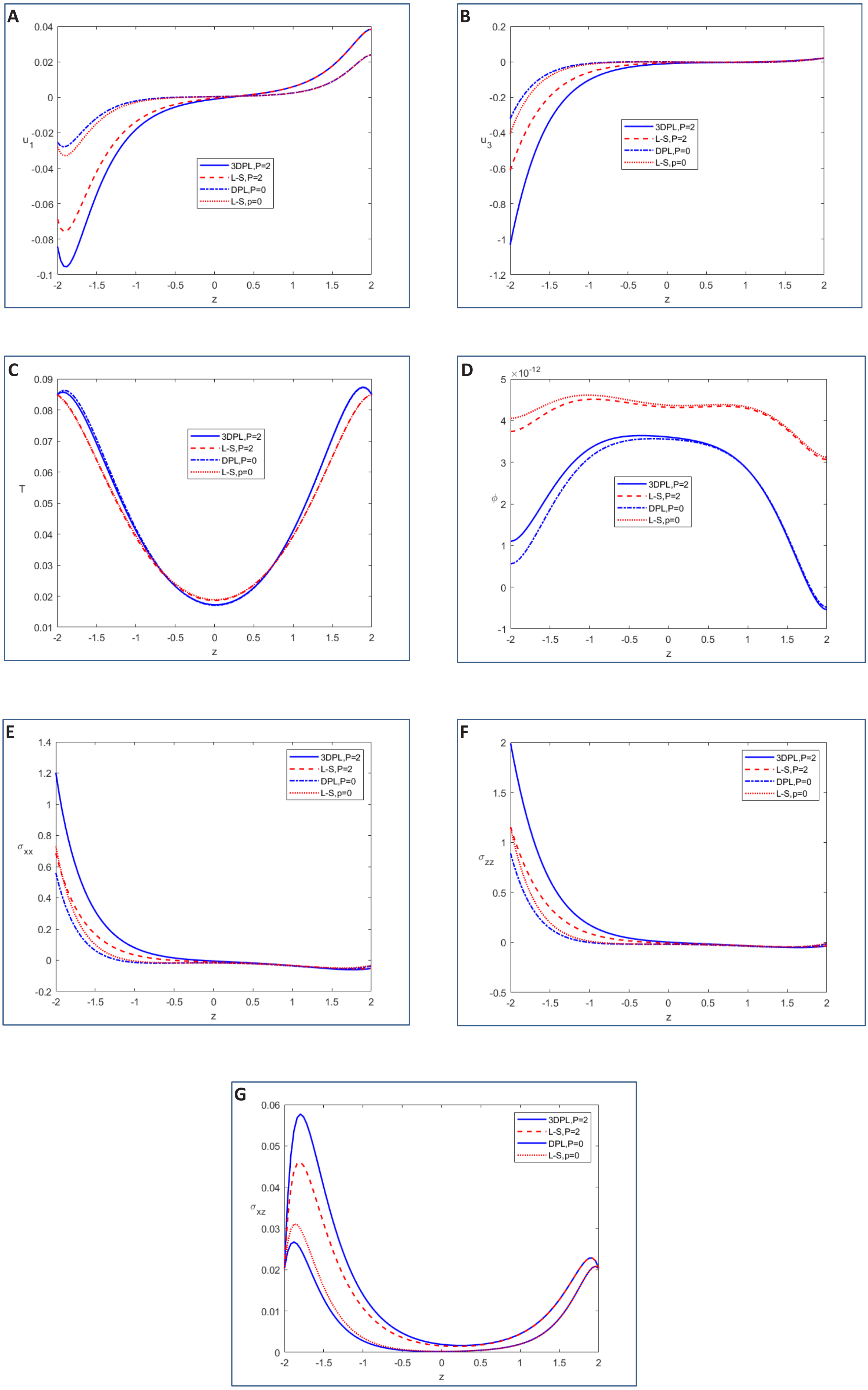

Figure 2. Variations of the Horizontal Displacement (A), Vertical Displacement (B), Temperature (C), Micro-elongational Scalar (D), and Force Stress Components (E-G) in the Presence and Complete Absence of Initial Stress.

Acknowledgements

Not applicable.

Conflicts of Interest

On behalf of all authors, the corresponding author states that there is no conflict of interest.

Data Availability

All data generated or analyzed during this study are included in this published article.

Author Contribution

All authors contributed to the study conception and design. Ismail MF and Ahmed KK performed the material preparation, data collection, and analysis. Emadifar H and Ahmed HM wrote the first draft of the manuscript. All authors commented on previous versions of the manuscript, read and approved the final manuscript.s

Abbreviation List

DPL, Dual-Phase-Lag
L-S, Lord-Shulman
ODEs, Ordinary differential equations
PDEs, Partial differential equations
p, Initial pressure
T, Absolute temperature
T_0, Reference temperature
a_0, λ_0, λ_1, Micro-elongational constants
c_1^f, Velocity of sound of fluid
c_e, Specific heat at the constant strain in micro-elongated medium
j_0, Microinertia
k, Thermal conductivity in micro-elongated medium
u, Displacement vector in micro-elongated medium
u^f, Displacement vector for fluid
$\alpha_{t_1}, \alpha_{t_2}$, Coefficient of linear thermal expansion where $\beta_0 = (3+2\mu)\alpha_{t_1}, \beta_1 = (3+2\mu)\alpha_{t_2}$
λ, μ, Lame's constants in micro-elongated medium
λ^f, Bulk modulus
ρ, Density in micro-elongated medium
ρ^f, Density of fluid
σ_{ij}, Component of stress tensor for micro-elongated medium
σ^f_{ij}, Component of stress tensor of fluid
τ_q, Heat flux parameter
τ_θ, Temperature gradient parameter
ϕ, Micro-elongational scalar

References

[1] Quintanilla R. Exponential stability in the dual-phase-lag heat conduction theory. *J Non-Equilib Thermodyn*, 2002; 27: 217-227. [DOI]

[2] Quintanilla R, Racke R. A note on stability in dual-phase-lag heat conduction. *Int J Heat Mass Transf*, 2006; 49: 1209-1213.[DOI]

[3] Quintanilla R, Racke R. Qualitative aspects in dual-phase-lag thermoelasticity. *SIAM J Appl Math*, 2006; 66: 977-1001.[DOI]

[4] RoyChoudhuri SK. One-dimensional thermoelastic waves in elastic half-space with dual phase-lag effects. *J Mech Mater Struct*, 2007; 2: 489-503.[DOI]

[5] Bayones FS, Kilany AA, Abo-Dahab SM et al. Electromagnetic field and rotation for fractional derivative order calculus with temperature-dependent on reflection of longitudinal wave under initial stress and three-phase-lag model. *Waves Random Complex Media*, 2025; 35: 1596-1616.[DOI]

[6] Elhag SH, Bayones FS, Kilany AA et al. Noninteger Derivative Order Analysis on Plane Wave Reflection from Electro-Magneto-Thermo-Microstretch Medium with a Gravity Field within the Three-Phase Lag Model. *Adv Math Phys*, 2022; 2022: 6559779.[DOI]

[7] Chen K, Hu Z, Xu Y. Thermal analysis of dual-phase-lag model in a two-dimensional plate subjected to a heat source moving along elliptical trajectories. *Int J Heat Mass Transf*, 2025; 244: 126880.[DOI]

[8] Sulaiman SA, Shomali Z. The non-local Dual Phase Lag model of heat conduction in a silicon metal-oxide-semiconductor field-effect transistor. *Int Commun Heat Mass Transf*, 2025; 165: 109034.[DOI]

[9] Kumar S, Meena BS. Computational Study on Single-Phase Lag and Dual-Phase Lag Bio-Heat Models of Heat Transfer in Irregular Tumors During Magnetic Nanoparticles Hyperthermia. *ASME J Heat Mass Transf*, 2025; 147: 064501.[DOI]

[10] Mukhtar NL, Jibril HM. Impact of Dual Phase Lag on Natural Convection Flow in a Porous Vertical Channel in the Presence of Periodic Boundary. *Heat Transf*, 2025; 54: 1623-1637.[DOI]

[11] Yahya A, Saidi A. Response of Generalized Thermoelastic for Free Vibration of a Solid Cylinder with Voids Under a Dual-Phase Lag Model. *Iran J Sci Technol Trans Mech Eng*, 2025; 49: 1333-1343.[DOI]

[12] Shaw S, Mukhopadhyay B. Periodically varying heat source response in a functionally graded microelongated medium. *Appl Math Comput*, 2012; 218: 6304-6313.[DOI]

[13] Shaw S, Mukhopadhyay B. Moving heat source response in a thermoelastic microelongated Solid. *J Eng Phys Thermophys*, 2013; 86: 716-722.[DOI]

[14] Ailawalia P, Sachdeva SK, Pathania DS. Plane strain deformation in a thermoelastic microelongated solid with Internal heat source. *Int J Appl Mech Eng*, 2015; 20: 717-731.[DOI]

[15] Ailawalia P, Sachdeva SK, Pathania DS. Internal heat source in thermoelastic microelongated solid under green lindsay theory. *J Theor Appl Mech*, 2016; 46: 65-82.[DOI]

[16] Ailawalia P, Singla A. A thermoelastic microelongated layer immersed in an infinite fluid and subjected to laser pulse heating. *Mech Mech Eng*, 2019; 23: 233-240.[DOI]

[17] Othman MIA, Tantawi RS, Eraki EEM. Effect of initial stress on a semiconductor material with temperature dependent properties under DPL model. *Microsyst Technol*, 2017; 23: 5587-5598.[DOI]

[18] Othman MIA, Atwa SY, Eraki EEM et al. Thermoelastic micro-stretch solid immersed in an infinite inviscid fluid and subject to gravity under three-phase-lag model. *Multidiscip Model Mater Struct*, 2023; 19: 21-37.[DOI]

[19] Umar M, Amin F, Al-Mdallal Q et al. A stochastic computing procedure to solve the dynamics of prevention in HIV system. *Biomed Signal Process Control*, 2022; 78: 103888.[DOI]

[20] Mukdasai K, Sabir Z, Raja MAZ et al. A numerical simulation of the fractional order Leptospirosis model using the supervise neural network. *Alex Eng J*, 2022; 61: 12431-12441.[DOI]

[21] Sadaf M, Arshed S, Akram G et al. Analytical investigation and graphical simulations for the solitary wave behavior of Chaffee–Infante equation. *Results Phys*, 2023; 54: 107097.[DOI]

[22] Shahzad A, Liaqat F, Ellahi Z et al. Thin film flow and heat transfer of Cu-nanofluids with slip and convective boundary condition over a stretching sheet. *Sci Rep*, 2022; 12: 14254.[DOI]

[23] Ali KK, Yusuf A, Yokus A et al. Optical waves solutions for the perturbed Fokas–Lenells equation through two different methods. *Results Phys*, 2023; 53: 106869.[DOI]

[24] Waqas H, Farooq U, Hassan A et al. Numerical and Computational simulation of blood flow on hybrid nanofluid with heat transfer through a stenotic artery: Silver and gold nanoparticles. *Results Phys*, 2023; 44: 106152.[DOI]

[25] Ali KK, Tarla S, Ali MR et al. Modulation instability analysis and optical solutions of an extended (2+1)-dimensional perturbed nonlinear Schrödinger equation. *Results Phys*, 2023; 45: 106255.[DOI]

[26] Zafar A, Raheel M, Mahnashi AM et al. Exploring the new soliton solutions to the nonlinear M-fractional evolution equations in shallow water by three analytical techniques. *Results Phys*, 2023; 54: 107092.[DOI]

[27] Razaq A, Hayat T, Khan SA et al. ATSS model based upon applications of Cattaneo-Christov thermal analysis for entropy optimized ternary nanomaterial flow with homogeneous-heterogeneous chemical reactions. *Alex Eng J*, 2023; 79: 390-401.[DOI]

[28] Khan SA, Razaq A, Alsaedi A et al. Modified thermal and solutal fluxes through convective flow of Reiner-Rivlin material. *Energy*, 2023; 283: 128516.[DOI]

[29] Hayat T, Alsaedi A, Razaq A et al. HARK formulation for entropy optimized convective flow beyond constant thermophysical properties. *Case Stud Therm Eng*, 2024; 54: 103983.[DOI]

[30] Khan SA, Razaq A, Hayat T. SAT formulation for entropy generated hybrid nanomaterial flow: Modified Cattaneo-Christov analysis. *Results Eng*, 2024; 24: 102895.[DOI]

[31] Hayat T, Razzaq A, Khan SA et al. TASA formulation for nonlinear radiative flow of Walter-B nanoliquid invoking microorganism and entropy generation. *Results Eng*, 2024; 24: 103346.[DOI]

[32] Ismail MF, Ahmed HM, El-Bary AA et al. Novel analytical wave solutions in nonlinear thermoelasticity using the IME tanh function method. *Int Commun Heat Mass Transf*, 2025; 166: 109044.[DOI]

[33] Othman MIA, Ismail MF. The gravitational field effect on a micro-elongated thermoelastic layer under a fluid load with two theories. *Multidiscip Model Mater Struct*, 2022; 18: 757-771.[DOI]